

Nanoparticle tracers in calcium carbonate porous media

Yan Vivian Li · Lawrence M. Cathles ·
Lynden A. Archer

Received: 7 March 2014 / Accepted: 25 June 2014 / Published online: 15 July 2014
© Springer Science+Business Media Dordrecht 2014

Abstract Tracers are perhaps the most direct way of diagnosing subsurface fluid flow pathways for ground water decontamination and for natural gas and oil production. Nanoparticle tracers could be particularly effective because they do not diffuse away from the fractures or channels where flow occurs and thus take much less time to travel between two points. In combination with a chemical tracer they can measure the degree of flow concentration. A prerequisite for tracer applications is that the particles are not retained in the porous media as the result of aggregation or sticking to mineral surfaces. By screening eight nanoparticles (3–100 nm in diameter) for retention when passed through calcium carbonate packed laboratory columns in artificial oil field brine solutions of variable ionic strength we show that the nanoparticles

with the least retention are 3 nm in diameter, nearly uncharged, and decorated with highly hydrophilic polymeric ligands. The details of these column experiments and the tri-modal distribution of zeta potential of the calcite sand particles in the brine used in our tests suggests that parts of the calcite surface have positive zeta potential and the retention of negatively charged nanoparticles occurs at these sites. Only neutral nanoparticles are immune to at least some retention.

Keywords Nanoparticle tracers · Stickiness · Zeta potential · Calcium carbonate · Porous media · Contaminants · Environmental effects

Electronic supplementary material The online version of this article (doi:[10.1007/s11051-014-2541-9](https://doi.org/10.1007/s11051-014-2541-9)) contains supplementary material, which is available to authorized users.

Y. V. Li (✉)
Department of Design and Merchandising, Colorado State University, Fort Collins, CO 80523, USA
e-mail: yan.li@colostate.edu

L. M. Cathles
Earth and Atmospheric Sciences, Cornell University, Ithaca, NY 14853, USA

L. A. Archer
School of Chemical and Biomolecular Engineering, Cornell University, Ithaca, NY 14853, USA

Introduction

Nanoparticles with novel mechanical, optical, biochemical, and catalytic properties have found special applications in a host of areas, including drug delivery (He et al. 2014), medical diagnosis (Bomati-Miguel et al. 2014), coatings (Zeng et al. 2013), electronics (Kang et al. 2014), energy (Wippermann et al. 2013), and the environment (Qian et al. 2013). Their high surface area provides an inherent mechanism for surface recognition and targeting using tethered molecules, as well as high carrying capacity per gram for drug delivery. Their small size, chemical reactivity, energy absorption, and biological mobility are

advantageous to medical diagnosis. Depending on their surface coating they can be superhydrophobic (Ling et al. 2009) or superhydrophilic (Liu and He 2008). They have been used to make smaller, faster, and more capable hand-held electrical devices (Mitrageotri 2013), and recently they have been used to make highly efficient battery electrodes (Lee et al. 2011). In subsurface flow applications, nanoparticles have been shown able to remove contaminants and toxic compounds from groundwater and produce clean water with significantly less cost, time, and labor (Savage and Diallo 2005). Nanoparticles have been found able to move contaminants adsorbed to them more quickly through the subsurface. Berlin et al. reported that oxidized carbon black functionalized with polyvinyl alcohol can carry a hydrophobic compound through a variety of oil-field rock types and release the compound where the rock contains hydrocarbon (Berlin et al. 2011).

It has been long recognized that large molecules or particles could in principle move significantly faster through the subsurface than chemical tracers because they do not diffuse into the surrounding rock from the fractures or permeable zones where the flow is occurring as chemical tracers would (Serres-Piole et al. 2012). In one of the earliest field test by Cathles et al. (1974) showed that a silica colloid tracer moved through a fractured igneous rock over 10 times faster than a simultaneously injected NaCl tracer. Becker and Shapiro (2000) offer an excellent review of the theoretical and experimental work that has been enabled by this dual-tracer methodology, showing that particles have not, to date, realized their tracer potential, largely because they are usually strongly retained as they pass through laboratory columns, rock cores, and rock and sediment formations.

The retention of nanoparticles in porous media has been found to depend on the size, shape, and surface chemistry of the particles, the water chemistry (pH, ionic strength, and valency of ions in solution) and porous media properties (pore size, fracture, and mineral chemistry; Frimmel et al. 2007). Colloidal silica has been shown to deposit in a partially reversible fashion on sand in a quartz sand media (Saiers et al. 1994). Pristine and surfactant-coated TiO₂ nanoparticles both showed strong stickiness when they were injected into quartz sand-packed columns, although the surfactant coating enhances the stability of the nanoparticles in solution (Godinez and

Darnault 2011). Brant et al. (2005) studied fullerene nanoparticles in aqueous systems and showed that they deposited on glass bead surfaces in a NaCl or NaOH solutions. Alaskar et al. (2011) studied the transport and mobility of fluorescent silica microspheres, silver nanowires, silver nanoparticles, tin–bismuth alloy nanoparticles, iron oxide Fe₂O₃ nanoparticles and polyvinyl pyrrolidone-coated iron oxide nanoparticles in porous and fractured media. These particles showed different degrees of stickiness to rock materials depending on the particle size and size distribution, shape, and surface charge (Cheraghian et al. 2014; Hamedi-Shokrlu and Babadagli 2014).

Some studies have identified particles that do not stick (Karimi et al. 2012; Villamizar et al. 2013). Rodriguez et al. (2009) showed that 20-nm silica nanoparticles with a coating that screens electrostatic attraction between the nanoparticle and the pore walls stay individually dispersed in water and pass easily through typical sedimentary rock pore throats. Agenet et al. (2012) demonstrated more than 95 % particle recovery in synthetic seawater coreflood experiments of easily detectable fluorescent silica nanoparticles in enhanced oil recovery. Yu et al. (2012) reported high particle recoveries when 2 % NaCl solutions containing the particles were passed through sandstone and dolomite cores, but found the particles were adsorbed when passed through limestone cores.

This paper reports screening experiments we carried out that identified small (<10 nm) and near zero charge carbon nanoparticles that show very low retention under extreme conditions. Subramanian et al. (2013) demonstrated in laboratory carbonate sand-packed column experiments that the best non-sticking nanoparticles function as an inert chemical tracer and when, referenced to a chemical tracer can measure of flow short-circuiting. These same particles showed 95 % recovery when passed through carbonate cores dispersed in oil field brine at 130 °C, and 86 % recovery when injected into the 130 °C Ghawar carbonate reservoir for several days and then retrieved (Kanj 2013). The particles also show low retention in low salinity laboratory experiments (Subramanian et al. 2013). We describe a screening methodology that efficiently evaluates the retention of all eight different nanoparticles when passed through columns containing crushed calcium carbonate sand. Retention is evaluated by analyzing the effluent particle concentration and calculating the fraction of the injected

particle mass that is retained in the column. Retention is found to be correlated with the ionic strength of the solution, particle size, and particle decoration. Slight retention of all the charged particles, together with other measurements, suggests the calcite sand particles have areas of positive as well as negative surface charge, and therefore that charged particles although mostly repelled, will always be attracted and retained to some degree. The work suggests that, contrary to some current common wisdom (Frimmel et al. 2007; Saiers et al. 1994), but in accord with some other recent studies as summarized above, small, slightly hairy particles with close to zero charge provide a robust platform for developing particle tracers with least retention for subsurface flow diagnosis and remediation.

Experimental section

Nanoparticle synthesis

Eight different nanoparticles were synthesized or purchased for this study, including three carbon-cored nanoparticles (CNPs) (Bourlinos et al. 2008; Krysmann et al. 2012), two silica-cored nanoparticles (SiNPs), two polymer (polystyrene, PSNP, and polyacrylonitrile, PANNP) nanoparticles, and one nanoparticle with a rare earth element core (CeNP).

The CNPs were synthesized using the method reported by Bourlinos et al. (2008) and Krysmann et al. (2012). A one-step thermal decomposition of citric acid (Sigma Aldrich) and polyetheramines (Jeffamine[®] M-1000, Huntsman) or ethanolamine (Sigma Aldrich) precursors was used to produce fluorescent CNP-1 and CNP-2 (and CNP-3) nanoparticles. The CNPs produced with the ethanolamine precursor were of two sizes (3.2 and 35.5 nm).

The two SiNPs consisted of a green fluorescent silica nanoparticle (SiNP-1) purchased from Corpu-scular Inc. (Cold Spring, NY, USA), and rhodamine-embedded silica nanoparticles (SiNP-2) synthesized in-house using standard sol-gel chemistry. The green SiNP-1 was received in a 2.5 % (by weight) aqueous solution. The particle size was 98 nm, as the manufacturer reported. SiNP-1 suspensions were prepared by diluting the stock suspension with deionized water from a Milli-Q system (Millipore) system to 0.01 %

(by weight) of nanoparticle tracer just prior to running the screening experiments. SiNP-2 was synthesized by coating silica seeds with dansyl chloride (Sigma Aldrich). Polyethylene glycol (PEG, Sigma Aldrich) was then grafted to the silica core to produce a PEG shell. The dansyl chloride made the SiNP-2 nanoparticles fluorescent.

The two polymer nanoparticles included polystyrene latex nanoparticles (PSNP) and polyacrylonitrile nanoparticles (PANNP). A 2 % (by weight) fluorescent polystyrene latex nanoparticle (Invitrogen[®]) was purchased from Life Technologies (Grand Island, NY, USA). The particle size was 100 nm, as the manufacturer reported. It was also diluted just prior to the screening experiments. Acrylonitrile (Sigma Aldrich) and Divinylpyrene (Sigma Aldrich) were used as precursors to synthesize polyacrylonitrile nanoparticles (PANNP). The vinylpyrene was incorporated in the polyacrylonitrile matrix to provide fluorescent properties. Cerium fluoride (CeF₃) nanoparticles were synthesized by adding a sodium fluoride (Sigma Aldrich) solution into a cerium chloride and terbium chloride solution. The synthesis for eight nanoparticles is illustrated in Fig. 1. Details of the synthesis methods of the nanoparticles made in our laboratory are discussed and given in Text S1 (Supplemental Material).

Nanoparticle fluorescence

The nanoparticle concentrations were determined by fluorescence spectrometry using a Molecular Devices SpectraMax M2^c. The injection concentrations were 60 ppm for the PANNP and 100 ppm for the other seven particles. Fluorescent excitation was at 360 nm for the CNP-1, CNP-2, CNP-3, and SiNP-2, at 515 nm for the SiNP-1, at 490 nm for the PSNP, and at 250 nm for the PANNP and CeNP. The fluorescent spectra of the eight NPs are shown in Fig. S1 (Supplementary Material). All three carbon-cored NPs (CNP 1–3) can be excited at 360 nm and show an emission peak at around 460 nm; however, the intensity of the emission peak is different. The ethanolamine nanoparticles CNP-2 and CNP-3 exhibit strong fluorescence even at 100 ppm (Bourlinos et al. 2008). The CNPs consist of a carbon core coated with amide fluorophores. The intense fluorescence is mainly due to the amide fluorophores although there is some fluorescence from the carbon core itself (Krysmann et al. 2012). CeNPs

Fig. 1 Synthesis scheme for the eight nanoparticles screened for transport through columns filled with crushed carbonate sands. The nanoparticles include organic (PSNP, PAVNP, CeNP), inorganic (SiNP-1), and organic–inorganic hybrid (CNPs, SiNP-2) particles

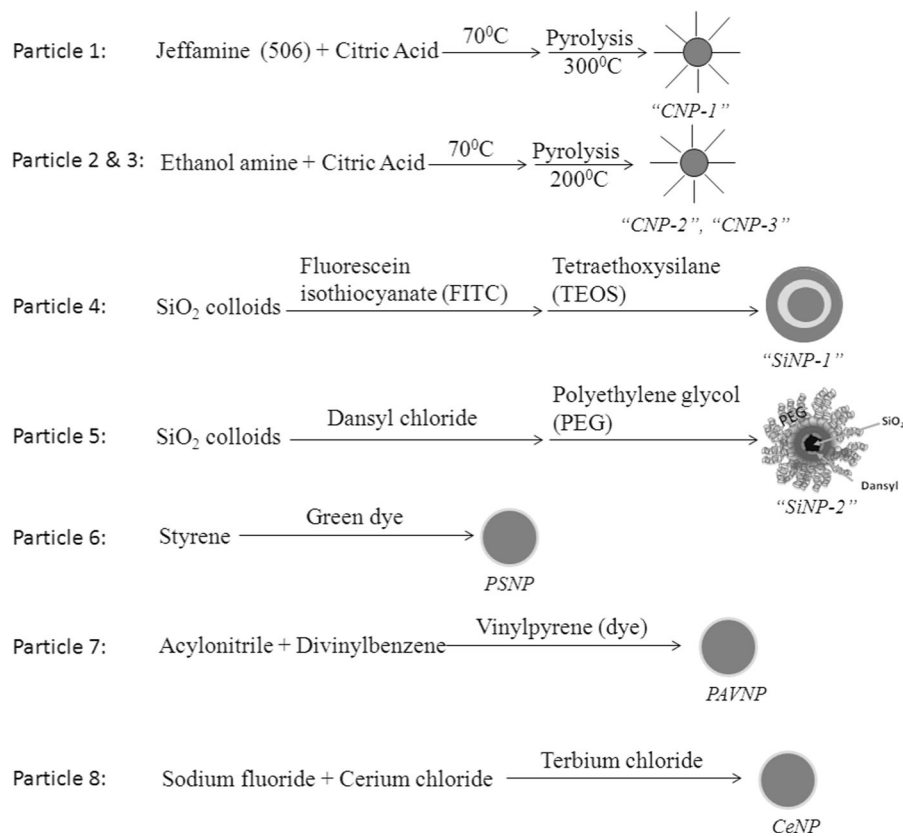


exhibit an intense Tb peak at 545 nm and two small peaks at 585 and 620 nm (van Krevel et al. 2002). The other particles (SiNP-1, SiNP-2, PSNP, PANNP) show emission around 500 nm, except for PANNP that shows emission at 320 nm.

For all the NPs, the peak emission intensity is a linear function of nanoparticle concentration at concentrations <100 ppm. The peak emission is used to produce a calibration curve of nanoparticle concentration versus fluorescence intensity.

Calcium carbonate sand

The calcium carbonate sand used in the study was obtained from Specialty Mineral Inc., Lucerne Valley, CA, USA. The properties of calcium carbonate sands are shown in Fig. S2 (Supplementary Material).

Particle size and zeta potential

Particle size and zeta potential for NPs and calcium carbonate sands in aqueous solutions were measured

with a Zetasizer Nano system (Malvern instrument Ltd.). The measurement is based on light scattering theory, and the zeta potential is deduced from the electrophoretic mobility of the particles measured by laser velocimetry.

Synthetic brine

The stickiness of NPs was investigated in pure water and brine. The brine composition was chosen to correspond roughly to oil field production water (Lindlof and Stoffer 1983). Three salts including NaCl, CaCl₂, and MgCl₂ were dissolved with concentrations of 128.9 g/L for NaCl, 109.2 g/L for CaCl₂, and 35.7 g/L for MgCl₂, respectively.

Screening column design

The screening column was home-built using a design described previously (Kanel et al. 2007; Jaisi et al. 2008; Godinez and Darnault 2011). The screening experiments were conducted by passing nanoparticles

Table 1 Particles size and zeta potential of eight NPs measured by Zetasizer

Particle	Size (nm)		Zeta potential (mV)		pH	
	In DI water	In brine	In DI water	In brine	In DI water	In brine
CNP-1	3.2 ± 1.0	3.1 ± 0.8	-2.5 ± 1.0	-2.0 ± 3.1	7.32	6.30
CNP-2	3.5 ± 2.1	3.3 ± 2.1	-1.5 ± 2.0	-0.88 ± 3.4	7.35	6.34
CNP-3	35.5 ± 10.3	35.2 ± 8.9	-3.0 ± 8.4	-4.4 ± 2.9	7.46	6.20
SiNP-1	68.1 ± 25.3	Precipitated	-35.5 ± 12.8	Precipitated	7.65	6.59
SiNP-2	21.5 ± 5.7	100.1 ± 23.7	-12.5 ± 4.5	-8.6 ± 5.5	7.82	6.50
PSNP	80.9 ± 15.4	Precipitated	-45.4 ± 12.3	Precipitated	7.39	6.20
PANNP	34.6 ± 6.7	120.3 ± 6.7	-24.9 ± 11.8	-15.7 ± 10.4	8.89	6.95
CeNP	32 ± 10	Precipitated	25.0 ± 15.0	Precipitated	-	-

Table 2 Zeta potential of calcium carbonate sand by Zetasizer

Solution	Zeta potential (mV)	pH
In DI water	-14.5 ± 5.2	8.44
In brine solution (2.21 M NaCl, 0.74 M CaCl ₂ , 0.18 M MgCl ₂)	-0.5 ± 4.7	6.03
In 2.21 M NaCl solution	-10.7 ± 4.1	7.54
In 0.74 M CaCl ₂ solution	5.2 ± 6.8	6.72
In 0.18 M MgCl ₂ solution	9.6 ± 2.1	8.82

and KBr solutions through a transparent polycarbonate column filled with calcium carbonate sands (see Fig. S3, Supplementary Material). The design of the column is described in Text S2 (Supplementary Material).

Fluid analysis

The concentration of nanoparticles in effluent samples was determined with a SpectraMax M2e spectrofluorometer (Molecular Devices, Inc., Sunnyvale, CA, USA). Before assessing effluent samples, a series of nanoparticle suspensions with known concentrations were prepared and a calibration curve relating fluorescent intensity to nanoparticle concentration was established. The fluorescence calibration curves were used to determine the concentration of nanoparticles in the effluent from each test. The chemical tracer used in the experiments as a reference was KBr (reagent grade purchased from ACROS). The concentration of KBr in effluent samples was determined with an Ion Selective Electrode connected to a pH/mV/Temp microprocessor handheld meter (6230N, Jenco Instruments). Prior to measuring the effluent concentration of KBr in each

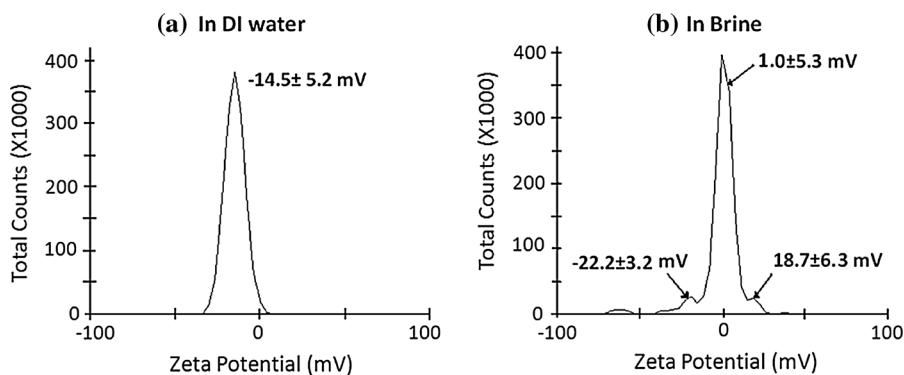


Fig. 2 Zeta potential distributions of calcium carbonate dispersed in **a** DI water and **b** in the synthetic mixed (2.21 M NaCl, 0.74 M CaCl₂, 0.18 M MgCl₂) oil field brine used in our experiments. **a** The zeta potential of calcium carbonate sand is

negative (-14.5 mV) in DI water and the distribution is monomodal. **b** For the mixed brine composition the zeta potential is close to zero (-0.5 ± 11.4 mV) but has a large spread and is trimodal

experiment, KBr solutions with known concentrations were prepared and a calibration curve of KBr concentration as a function of electrode offset voltage determined. The KBr concentration injected in all the experiments was 500 ppm. The protocol of our fluid analysis is given in Text S3 (Supplementary Material).

SEM observations

Scanning electron microscopy (LEO 1550 FESEM) was used to examine particle residues on the calcium carbonate sand after completion of the column tests. After flushing was terminated, samples of calcium carbonate sand were taken out of the columns at the inlet end, dried, and examined for nanoparticle residues.

Results and discussion

Particle size and zeta potential

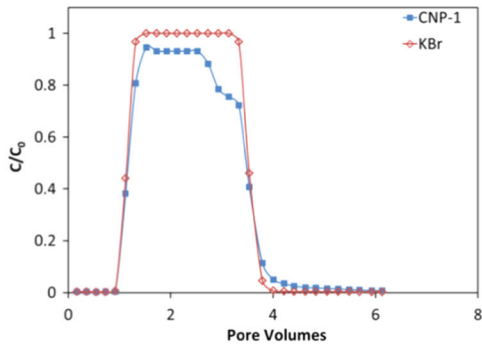
The sizes of all the NPs in DI water and in brine measured with the Zetasizer are shown in Table 1. In DI water all are smaller than 100 nm, which is important because particles larger than 100 nm may not remain mobile in natural porous media (Kanj 2013). Nanoparticles <100 nm avoid direct plugging and bridging in the micro pore network systems commonly encountered in the subsurface, according to the size exclusion principle. However, except for carbon-cored nanoparticles (CNP-1, CNP-2, and CNP-3), salinity has great impact on the particle size. When SiNP-2 and PANNP particles are dispersed in brine, the particles aggregate to form clusters whose size is about 5 times larger than the size measured in DI water. The other three particles (SiNP-1, PSNP, and CeNP) also aggregate significantly, and the precipitation can even be seen in the solution.

Even if they do not aggregate, the smaller nanoparticles can still interact with other particles or stick to mineral surfaces. If the particles are charged, electrostatic interactions are an important factor controlling particle interactions with mineral surfaces. The zeta potential (the electric potential at a distance from the particle at which water moves past the particle, called the slipping plane) is the most practical way to measure particle charge. Table 1 shows the zeta potentials for the eight particles in DI water and in

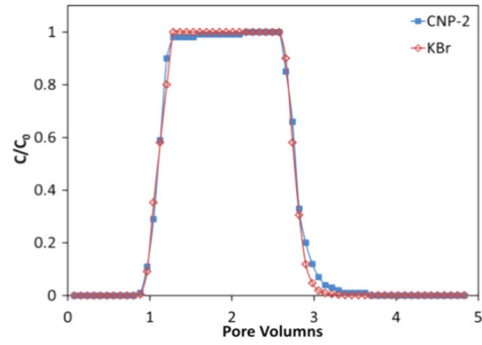
Fig. 3 The ratio of collected to injected NPs (blue) and KBr (red) concentration as a function of injection pore volume when the particles were dispersed in DI water. No significant particle retention was found for CNP-2 (b), CNP-3 (c), SiNP-1 (d), SiNP-2 (e), and PANNP (g), as indicated by the overlap of the nanoparticles and KBr tracer arrival curves. Two nanoparticles, CNP-1 (a) and PSNP (f), stick only very slightly (11.5 % and 15.2 %, respectively retention). One particle was very sticky. The CeNP (h), particle showed 99 % retention. (Color figure online)

brine. In DI water, only the CeNP particles are positively charged; the rest are negatively charged. The absolute values of negative zeta potential of CNP-1 and CNP-2 particles are closer to zero than the other five negatively charged nanoparticles, suggesting that CNP-1 and CNP-2 are nearly neutral, and that electrostatic force on these particles will be small. When the particles are suspended in brine (2.21 M NaCl, 0.74 M CaCl₂, 0.18 M MgCl₂), the zeta potentials of the carbon-cored nanoparticles are not changed significantly. However, zeta potentials of the SiNP-2 and PANNP particles become less negative.

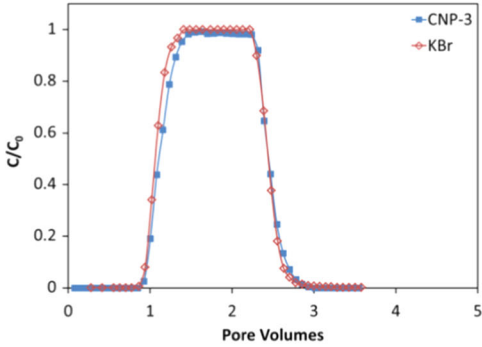
The zeta potential of calcium carbonate sand in various solutions is shown in Table 2. The zeta potential of calcium carbonate sand is negative (−14.5 mV) in DI water and the distribution is mono-modal, as shown in Fig. 2a. In non-dilute solutions, the calcite zeta potential depends strongly on brine composition. Table 2 shows that in pure NaCl brine the zeta potential of calcium carbonate particles is -10.7 ± 4.1 mV, whereas in pure CaCl₂ and MgCl₂ brines the zeta potential is 5.2 ± 6.8 and 9.6 ± 2.1 mV, respectively. For the mixed brine composition that simulates oil field brines that we use in our experiments (see composition above) the zeta potential is close to zero (-0.5 ± 11.4 mV) but has a large spread and is tri-modal as shown in Fig. 2b. The primary peak is at 1.0 mV and has a spread of ± 5.3 mV, but there are two secondary peaks at 18.7 ± 6.3 mV and at -22.2 ± 3.3 mV. The secondary peaks suggest that although most of the calcite particles have zeta potentials near zero, some of the particles may have positive and some negative zeta potentials. We have been unable to determine the zeta potential distributions for the pure brine solutions. The Zetasizer reports only the peak and its spread and does not give the distribution plot. But this interpretation of a zeta potential distribution is compatible with the particle retention experiments described in the next sections.



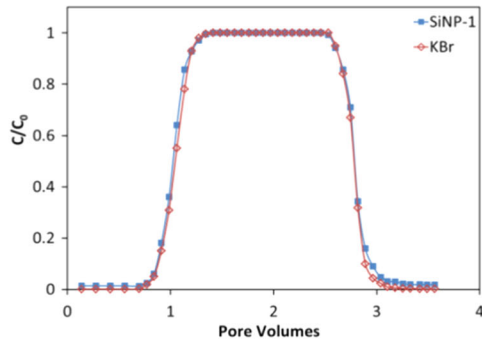
(a) 2.5 PV of CNP-1/KBr solution injected



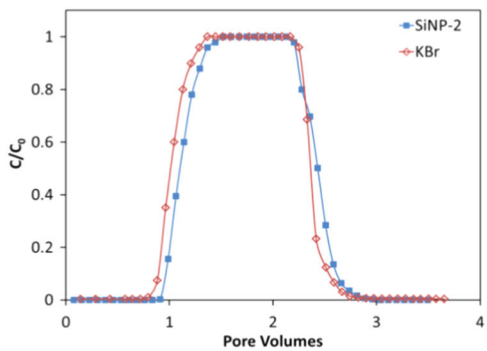
(b) 2.0 PV of CNP-2/KBr solution injected



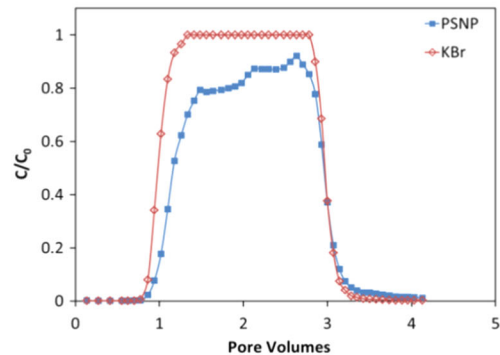
(c) 1.5 PV of CNP-3/KBr solution injected



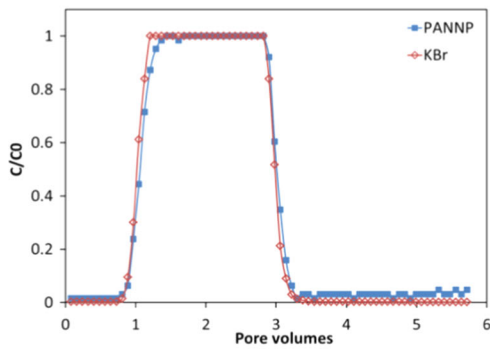
(d) 1.7 PV of SiNP-1/KBr solution injected



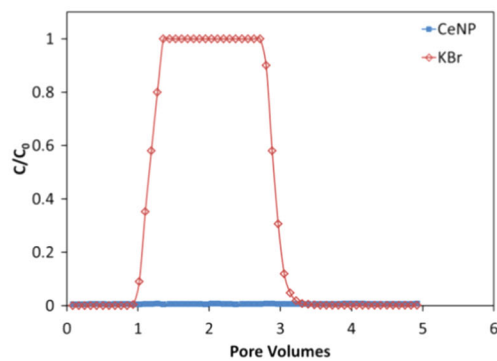
(e) 1.4 PV of SiNP-2/KBr solution injected



(f) 2.0 PV of PSNP/KBr solution injected



(g) 2.0 PV of PANNP/KBr solution injected



(h) 1.9 PV of CeNP/KBr solution injected

Nanoparticle transport in deionized water

Figure 3a shows the effluent concentration of CNP-1 and KBr dissolved in distilled water solution as a function of the number of pore volumes of fluid injected through the column. Tracer breakthrough starts at 0.9 PV. While the Br tracer concentration rapidly rises to $C/C_0 = 1$, the rise in CNP-1 concentration slows down after $C/C_0 \sim 95\%$ and the plateau is not flat. We interpret the differences between the tracer curves for CNP-1 and KBr to indicate partial sticking or attachment of the CNP-1 on the calcium carbonate sand surface. The attachment of CNP-1 is strong enough that the attached CNP-1 particles are not washed off after 3.5 PV of water flushing.

Figure 3b, c, d, g show the concentration history of CNP-2, CNP-3, SiNP-1, and PANNP. The arrival curves of these four NPs are quite similar to the KBr tracer injected with them, indicating very little retention of these four NPs in the column. The CNP-2, CNP-3, SiNP-1, and PANNP particles are not sticking to the water-wet calcium carbonate sand, and are not retained in the column in any other fashion.

Figure 3e shows the breakthrough of SiNP-2 is 0.1 PV later than that of simultaneously injected KBr tracers. There is a similar delay in the termination of the nanoparticle compared to the KBr tracer. The delay in the particle arrival indicates that a small portion of SiNP-2 is captured in the porous media at the beginning of injection. The delay in the arrival of particle-free flushing water indicates that the particles are not trapped permanently because they are recovered by the later flushing. It is unlikely that the particles are temporarily sequestered in dead end pores because there is no delay for the SiNP-1 particle (or the CNP or PANNP particles). The SiNP-1 and SiNP-2 are both silica-cored particles, but there are flexible polymeric chains (polyethylene glycol) grafted to the SiNP-2 cores whereas the SiNP-1 particles are bare SiO_2 . The polymeric chains, therefore, appear to be responsible for the slight sticking of the SiNP-2 particle to the calcium carbonate sand surface of the porous media.

Figure 3f shows the effluent concentration history of the polystyrene nanoparticles. The breakthrough of PSNPs starts at around 1 PV, as does the KBr tracer, but the arrival of the PSNPs concentration is substantially delayed compared to the KBr and does not reach

Fig. 4 The ratio of collected to injected NPs concentration as a function of injection pore volume when the particles were dispersed in brine. No KBr tracer was injected because the presence of ions (Na^+ , Ca^{2+} , Mg^{2+} , and Cl^-) interfere with the measurement of Br^- concentration. High particle recovery (more than 99 %) was only found in CNP-2 (b). Three particles including SiNP-1 (d), SiNP-2 (f), and CeNP (h) were very sticking and were retained significantly in brine saturated column. Other particles were retained in the column to different degree: CNP-1 (a), CNP-3 (c), SiNP-1 (d), and PANNP (g)

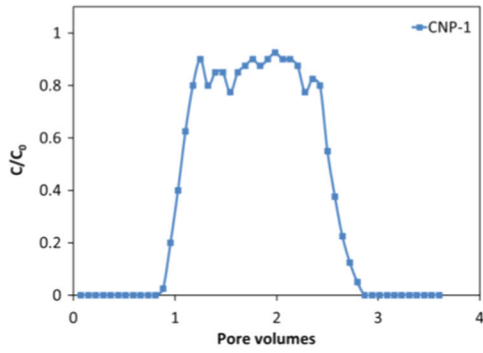
the injected concentration. The maximum concentration of PSNPs is only 92 %. Only a small fraction of the retained particles are flushed out. This suggests that some of PSNPs are attaching to the calcium carbonate sand surface and are not washed off after 2 PV of water flushing.

It is apparent from Fig. 3 that distinctly different concentration histories and styles of retention are exhibited by the various nanoparticle tracers. The functionalized silica nanoparticles (SiNP-2 in Fig. 3e) stick only slightly and are easily flushed. The Jeffemine-functionalized carbon nanoparticles (CNP-1 in Fig. 3a) are increasingly retained with continued injection (e.g., downward slope to their maximum effluent concentration) as if the particles are becoming increasingly tangled. By contrast the polystyrene nanoparticles (PSNP in Fig. 3f) are decreasingly retained with continued injection as if the available sites for retention are becoming increasingly occupied.

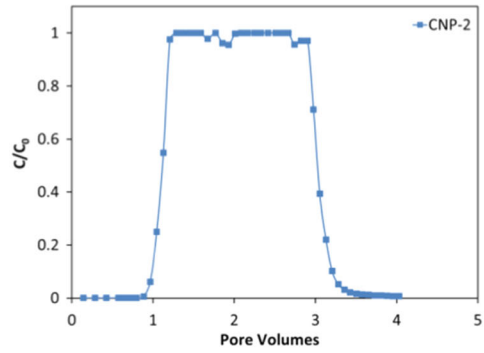
The concentration history of CeNP particles is shown in Fig. 3h. The effluent concentration is close to zero during the entire injection and flushing histories (5 PV in total). The CeNP particles, therefore, appear to stick completely to the calcium carbonate sand surface and the attachment is strong. This is anticipated from the positive zeta potential of these particles and the negative zeta potential of the calcium carbonate sand surface. There should be a strong electrostatic attraction between the particles and the calcium carbonate sand and this should result in strong and irreversible adhesion.

Nanoparticle transport in brine solutions

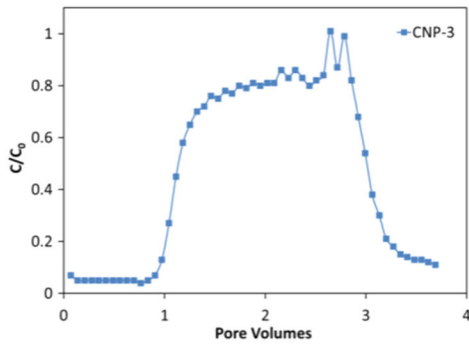
When the NPs are suspended in brine solutions, their transport behaviors are different from when they are suspended in distilled water. The high concentrations of ions (Na^+ , Ca^{2+} , Mg^{2+} , and Cl^-) have a significant impact on the NPs transport behavior. Figure 4 shows the effluent concentration histories of NPs dispersed in



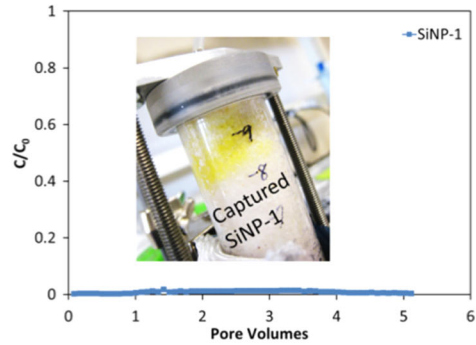
(a) 1.5 PV of CNP-1 solution injected



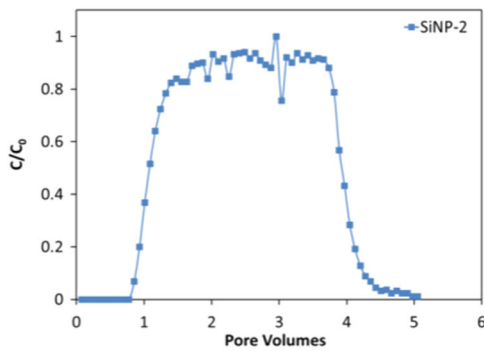
(b) 2 PV of CNP-2 solution injected



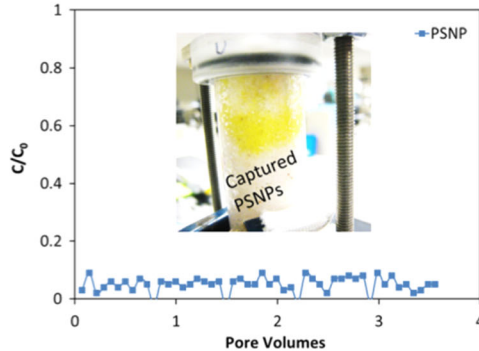
(c) PV of CNP-3 solution injected



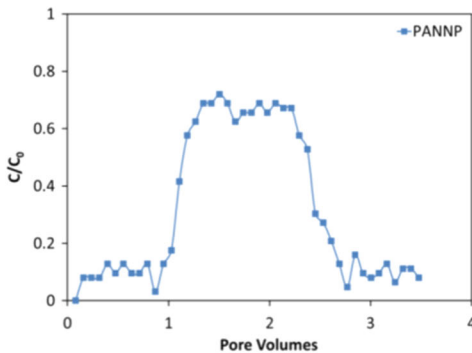
(d) 1.5 PV of SiNP-1 solution injected



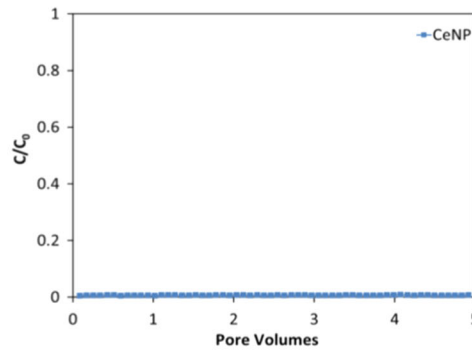
(e) PV of SiNP-2 solution injected



(f) 1.5 PV of PSNP solution injected



(g) 1.5 PV of PANNP solution injected



(h) 2 PV of CeNP solution injected

brine and passed through the calcium carbonate sand-packed column. No KBr tracer was injected at the same time because the presence of ions (Na^+ , Ca^{2+} , Mg^{2+} , and Cl^-) interfered the measurement of Br^- concentration. The two commercial SiNP-1 and PSNP particles exhibit very poor stability in brine solutions (Fig. 4d, f). These particles are completely, or nearly completely, retained in the column. The yellow color in the insert pictures in Fig. 4d, f show the SiNP-1 and PSNPs are attached to the calcium carbonate sand, especially near the inlet (top part of tube in the picture). This is not surprising because the particles precipitated when simply dissolved in brine as noted in Table 1. The CeNPs are also not mobile in the brine as shown in Fig. 4h and as noted in Table 1.

Figure 4a, c, e, g show that most of CNP-1, CNP-3, SiNP-2, and PANNP NPs are mobile enough to be recovered in the column effluent. The maximum concentrations in effluents for these four NPs are approximately in the range of 74–87 %. The non-stickiness of the ethanolamine functionalized carbon-cored nanoparticles is striking in contrast to the others. Figure 4b shows that the concentration history of CNP-2 closely follows that of the KBr tracer, indicating that there is little retention of these particles even when they are injected in brine.

The SEM images of CNP-3 and PSNP particles retained on the calcium carbonate sand surface after the brine experiments are shown in Fig. 5. The inset in Fig. 5b illustrates PSNP clusters of aggregated particles, which is not the case for CNP-3 in Fig. 5a. The CNP-3 (35.5 ± 10.3 nm in diameter) is smaller than PSNP (80.9 ± 15.4 nm in diameter). This size dependence of particle aggregation was also reported previously for silver nanoparticles in electroless fabrication process (Gentile et al. 2012). They

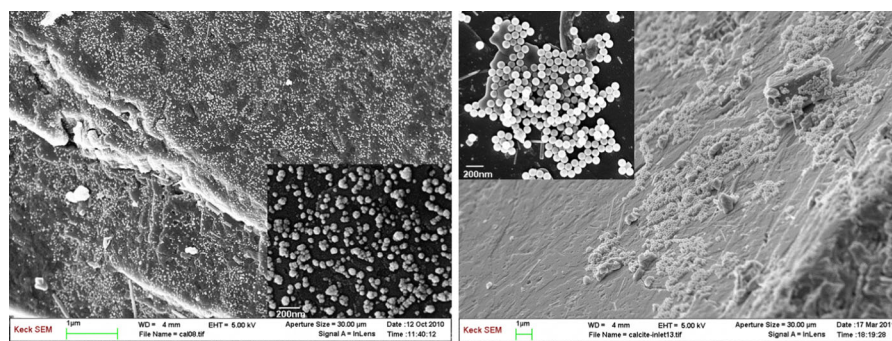
explained that larger particles were more discontinuous than smaller. The retention of all the larger particles is visually confirmed by the SEM images that show particles adhering to the calcite surface (see Figure S4, supplementary material). The SEM images are discussed in Text S4 (Supplementary Material). The CNP-1 and CNP-2 particles are too small to be seen by the SEM and so we cannot confirm the slight retention of the CNP-1 particles or the lack of retention of the CNP-2 particles from SEM observations.

Nanoparticle stickiness

The concentration histories of KBr in all the effluents in Fig. 3 are similar. The ions of Br exhibit Brownian motion in a wet and homogeneous porous media. They diffuse completely in the pores and fully fill the simple geometric pore space in the column. The symmetric shape of the concentration history curve of KBr as shown in Fig. 3 confirms the diffusion behavior of the ion. The CNP-2, CNP-3, SiNP-1, and PANNP particles exhibit very similar behavior to the Br⁻ in the same calcium carbonate sand-packed column, suggesting they show neither stickiness to the calcium carbonate sand nor sequestration in the column. However, the CNP-1, PSNP, SiNP-2, and CeNP particles exhibit different behaviors. The CNP-1 and PSNP particles are partially sticky, and almost 100 % of CeNP particles are retained in the column. These sticky particles are not removed by flushing. On the other hand, the breakthrough of the SiNP-2 particles is slightly delayed, compared with the Br ions, but later the particles are completely retrieved.

Figure 6 shows how the fraction of nanoparticles recovered from the column (obtained by integrating the area under the effluent curves in Figs. 3 and 4, and

Fig. 5 SEM images of CNP-3 (a) and PSNP (b) residues on calcium carbonate sand surfaces after brine-wet column tests. The insets show high-resolution images of a portion of the surface. The particle retention was significant for both CNP-3 and PSNP



(a) CNP-3

(b) PSNP

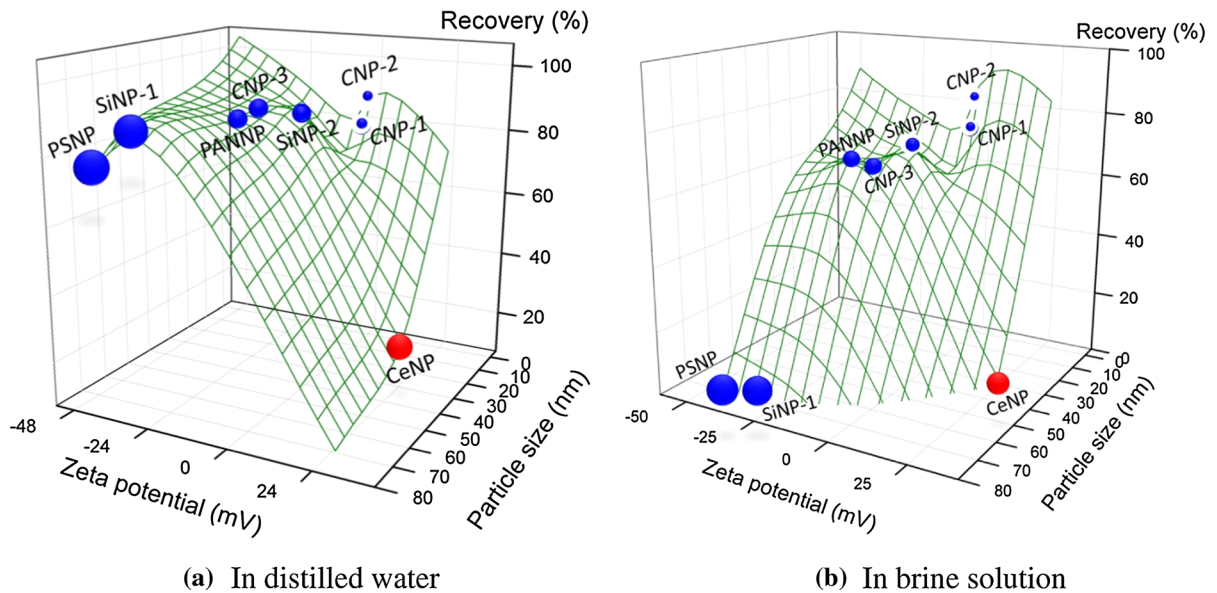


Fig. 6 3D-countour plots of particle recovery as a function of particle size (shown by the size of the circle) and zeta potential (blue negative, red positive) **a** in aqueous solution and **b** in brine solution. Most of nanoparticles screened in the experiments

dividing by total volume of nanoparticles injected) is related to size and zeta potential of the nanoparticles. In distilled water (Fig. 6a), the particles all exhibit high recovery (>80 %), except for the positively charged CeNPs. There is little difference in the total recovery for NPs with negative zeta potential. The simple explanation is that the negative charge of the nanoparticles keeps them in solution and away from the negatively charged calcium carbonate sand surface (see Table 2). The CeNP particles are retained because their positive charge attracts them to the surfaces of the calcium carbonate sand.

In brine solution the interactions between the nanoparticles and the calcium carbonate sand becomes more complex and the particles show different behaviors. Figure 6b shows a more varied recovery of the eight particles. Complete non-stickiness with calcium carbonate sand is found only for the CNP-2 particles. The other seven particles exhibit different degrees of stickiness to calcium carbonate sand surfaces.

Comparing the CNP-1, 2, and 3 particles, we see that smaller nanoparticles with near zero charge exhibit the highest recovery. In strong contrast to the zero recovery of SiNP-1, the SiNP-2 particles show

exhibit high particle recovery when dispersed in DI water, but low recovery when dispersed in brine. Only the CNP-2 particle shows little stickiness to the calcite surface in both DI water and brine conditions. (Color figure online)

72 % recovery. The polymeric hairs (PEG) attached to the SiNP-2 particles, that were a slight detriment to stability at low salinity, dramatically improve the stability of this particle in brine solution. Enhancement of particle stability by grafting polymer molecules (called steric stabilization) has been reported by others (Berlin et al. 2011; Alaskar et al. 2011; Rodriguez et al. 2009; Baez et al. 2012).

The influence of solution salinity on particle retention is shown dramatically by the difference in the tracer curves in Figs. 3 and 4 and by the drop in retention in the brine solution shown in Fig. 6. In DI water, all the particles except the positively charged CeNP show low retention, but in brine the larger particles are completely retained, and the smaller particles, except for the CNP-2, show substantial retention. The large particles aggregate and precipitate from solution so rapidly that their size and zeta potential cannot be measured (see Table 1). The smaller SiNP-2 and PANNP particles aggregate in brine to form clusters five times larger than the particles measured in DI water (see Table 1). The clusters are still dispersible but have less negative zeta potentials than in DI water. That the zeta potential of the calcium carbonate sand becomes increasingly

positive as the ionic strength of the brine increases agrees with the results of John (1973) and Lim et al. (2005), who measured and simulated the effective charge on a particle surface as a function of ionic strength and concluded that the effective charge decreases with increasing ionic strength. Decreasing charge should reduce electrostatic repulsion and particle stability (Menon and Zydney 1999), and so it is not surprising that these particles should aggregate and show more retention when passed through the column in brine solutions.

But in addition to the general decrease in zeta potential with increasing ionic strength, the zeta potential of calcium carbonate sand, which was mono-modal at -14.5 ± 5.2 mV in DI water, develops a tri-modal distribution in brine. The zeta potential distribution is such that most of the calcite particle in the packed column have near zero zeta potential, but some have very negative (-22.2 ± 6.3 mV) and some very positive (18.7 ± 3.3 mV) zeta potentials. This distribution could explain why nanoparticles with negative zeta potential (such as PANNP, CNP-3, SiNP-1 and CNP-1) show slight retention in brine solutions. They are attracted to the calcite sand particles, or portions of them, that have positive charge. That the zeta potential can be positive or negative depending on the proportion of the active ions (Na^+ , Cl^- , Ca^{2+} , Mg^{2+}), as we show in Table 2, has been reported previously by Douglas and Walker (1950), Smallwood (1977), and Hirasaki and Zhang (2004). Hirasaki and Zhang (2004) found that the zeta potential of calcium carbonate sand in a $\text{NaCl}\text{-Na}_2\text{CO}_3\text{-NaHCO}_3$ brine was close to zero (-0.1 mV at pH 9).

Particle charge is clearly important, but charge is not the whole story because the CNP-1, 2, and 3 nanoparticles are all similarly charged but the CNP-2 particle shows significantly less retention. Small particles may stick less than larger particles. The small CNP-2 particles (3 ± 2 nm) are retained less in the brine experiments (96 % recovery) than the larger CNP-3 (35 ± 10 nm) particles that showed 75 % recovery. Lecoanet et al. (2004) compared the mobility of small silica nanoparticles (57 nm in diameter) and large silica nanoparticles (135 nm in diameter) that were injected in glass bead packed column. Small silica particles (maximum effluent $C/C_0 = 97$ %) exhibited a higher mobility than the large particles ($C/C_0 = 68$ %).

Surface functionalization seems also to be important. The size of CNP-1 and CNP-2 is similar, but the surface functionality is different. The CNP-2 particles show the least retention and they are decorated or functionalized with highly hydrophilic polymer hairs derived from ethanolamine (Krysmann et al. 2012). The CNP-1 particles are functionalized with Jeffamine, which is slightly less hydrophilic than the ethanolamine due to its longer carbon chain. Rodriguez et al. (2009) noted that aqueous suspension of silica nanoparticles coated with polyethylene glycol (5–20 nm in diameter) injected into sedimentary rocks showed higher mobility and recovery than the bare silica nanoparticles. Kanel et al. (2007) found iron nanoparticles modified with non-ionic surfactant (polyoxyethylene sorbitan monolaurate) fully dispersed in aqueous solution and were completely recovered after being injected in a sand-packed column. Surface modifications that increase the hydrophilicity of the particles thus appear to reduce particle retention in porous media. The reduced retention could be because the polymer decoration keeps the particles far enough from the calcite surface that Van der Waals forces are not significant, or because the hydration forces that arise as water molecules are pulled into the gap between the particles and the surface keep the particles separated from the surface.

There are implications of what we report here that we will follow up in subsequent papers. Table 2 shows that the surface charge of calcium carbonate in brine solutions depends on the brine composition. Specifically, the zeta potential can be positive or negative depending on the proportion of the active ions (Na^+ , Cl^- , Ca^{2+} , Mg^{2+}). We propose that the wide range of zeta potentials for calcium carbonate measured in the mixed composition brine that we used in the experiments reported here suggests that some of the particles (or portions of the particles) had positive and some had negative zeta potential. Thus parts of the surface could attract and bind negatively charged nanoparticles whereas other parts would not. Under these circumstances, only zero charge particle could be immune to adsorption to all parts of the surface. Since the zeta potential of calcite in DI water is mono-modal and strongly negative, an implication of the mixed charge hypothesis is that particles retained in a brine experiment will be released if the column is

flooded with DI water. We have found this in fact to be the case, and this will be presented and discussed fully in a second paper that is now in the advanced stages of preparation.

Conclusions

We measured the retention of carbon-cored, silica, polymer, and rare earth element nanoparticles passed through columns packed with calcium carbonate sand in dilute and brine solutions. In aqueous solution, five of the particles exhibited more than 95 % total recovery, but only the carbon-cored and polymer-decorated CNP-2 particles with near zero zeta potential showed more than 95 % total recovery in the high salinity solution. Solution salinity promotes particle aggregation for the SiNP-2 and PANNP particles and precipitation of the SiNP-1, PSNP, and CeNP particles. The SiNP-1, PSNP, and CeNP particles are completely retained in the calcium carbonate sand-packed column when passed through in brine solutions.

Retention of the SiNP-2 and PANNP particles in brine solution probably result from the electrostatic attraction between the negative zeta potential of particle clusters and parts of the calcium carbonate sand surface with positive zeta potential. The zeta potential of most of the calcite surface is near zero in the mixed composition brine (2.21 M NaCl, 0.74 M CaCl₂, 0.18 M MgCl₂) that approximates oil field brine in our experiments, but parts of the calcite surface have positive zeta potentials to which negatively charged particles are attracted. The particles that show the least retention have a near zero zeta potential, and are small and protected from close contact with the carbonate surface by virtue of their being decorated with highly hydrophilic polymer hairs. A similar size particle with less hydrophilic decoration shows more retention, suggesting hydration forces may provide additional protection from sticking (e.g., in addition to steric forces provided by the polymer hairs). A smaller particle is less retained than a larger one with identical decoration. The experimental results reported here thus suggest that most non-interacting nanoparticles, and the best candidates for tracer nanoparticles, may be small particles with zero charge and a highly hydrophilic polymer decoration.

Acknowledgments This publication is based on work carried out with collaboration and support from Aramco Services Company (Project ID: ASC #660022190), for which we are most grateful. Facilities and minor support came also from Award No. KUS-C1-018-02 from the King Abdullah University of Science and Technology. Additional support was provided from general funding to L. Cathles from The International Research Institute of Stavanger.

Conflict of interest The authors declare no competing financial interest.

References

- Agenet N, Perriat P, Bricart T, Crowther N, Martini M, Tillement O (2012) Fluorescent nanobeads: a first step toward intelligent water tracers. Society of Petroleum Engineers, SPE-157019-MS. doi:[10.2118/157019-MS](https://doi.org/10.2118/157019-MS)
- Alaskar M, Ames M, Connor S, Liu C, Cui Y, Li K, Roland H (2011) Nanoparticle and microparticle flow in porous and fractured media: an experimental study. In: 2011 society of petroleum engineers (SPE) annual technical conference and exhibition, Denver, Colorado, USA, SPE-146752-PA. doi:[10.2118/146752-PA](https://doi.org/10.2118/146752-PA)
- Baez JL, Ruiz MP, Faria J, Harwell JH, Shiau B, Resasco DE (2012) Stabilization of interfacially-active-nanohybrids/polymer suspensions and transport through porous media. In: The eighteenth SPE improved oil recovery symposium, society of petroleum engineers, Tulsa, Oklahoma, USA, SPE-154052-MS, doi:[10.2118/154052-MS](https://doi.org/10.2118/154052-MS)
- Becker MW, Shapiro AM (2000) Tracer transport in fractured crystalline rock: evidence of nondiffusive breakthrough tailing. *Water Resour Res* 36(7):1677–1686
- Berlin JM, Yu J, Lu W, Walsh EE, Zhang L, Zhang P, Chen W, Kan AT, Wong MS, Tomson MB, Tour JM (2011) Engineered nanoparticles for hydrocarbon detection in oil-field rocks. *Energy Environ Sci* 4:505–509
- Bomati-Miguel O, Miguel-Sancho N, Abasolo I, Candiota A, Roca A, Acosta M, Schwartz S Jr, Arus C, Marquina C, Martinez G, Santamaria J (2014) Ex vivo assessment of polyol coated-iron oxide nanoparticles for MRI diagnosis applications: toxicological and MRI contrast enhancement effects. *J Nanopart Res* 16(3):1–13
- Bourlinos AB, Stassinopoulos A, Anglos D, Zboril R, Karakassides M, Giannelis EP (2008) Surface functionalized carbogenic quantum dots. *Small* 4(4):455–458
- Brant J, Lecoanet H, Wiesner MR (2005) Aggregation and deposition characteristics of fullerene nanoparticles in aqueous systems. *J Nanopart Res* 7(4):545–553
- Cathles LM, Spedden HR, Malouf EE (1974) A tracer technique to measure the diffusional accessibility of matrix block mineralization. In: 103rd AIME annual meeting, the American Institute of Mining, 73-94005
- Cheraghian G, Hemmati M, Masihi M, Bazgir S (2014) An experimental investigation of the enhanced oil recovery and improved performance of drilling fluids using titanium dioxide and fumed silica nanoparticles. *J Nanostruct Chem* 3(1):78

- Douglas HW, Walker RA (1950) The electrokinetic behaviour of Iceland spar against aqueous electrolyte solutions. *Trans Faraday Soc* 46:559–568
- Frimmel FH, Kammer F, Flemming H-C (2007) *Colloidal transport in porous media*. Springer, New York
- Gentile F, Coluccio ML, Toma A, Rondonina E, Leoncini M, De Angelis F, Das G, Dorigoni C, Candeloro P, Di Fabrizio E (2012) Electroless deposition dynamics of silver nanoparticles clusters: a diffusion limited aggregation (DLA) approach. *Microelectron Eng* 98:359–362
- Godinez IG, Darnault CJG (2011) Aggregation and transport of nano-TiO₂ in saturated porous media: effects of pH, surfactants and flow velocity. *Water Res* 45:839–851
- Hamedi-Shokrlu Y, Babadagli T (2014) Stabilization of nano-metal catalysts and their interaction with oleic phase in porous media during enhanced oil recovery. *Ind Eng Chem Res* 53(20):8464–8475
- He L, Huang Y, Zhu H, Pang G, Zheng W, Wong Y-S, Chen T (2014) Drug delivery: cancer-targeted monodisperse mesoporous silica nanoparticles as carrier of ruthenium polypyridyl complexes to enhance theranostic effects. *Adv Funct Mater* 24(19):2737
- Hirasaki G, Zhang DL (2004) Surface chemistry of oil recovery from fractured, oil-wet, carbonate formations. *Soc Petrol Eng J* 9(2):151–162
- Jaisi DP, Saleh NB, Blake RE, Elimelech M (2008) Transport of single-walled carbon nanotubes in porous media: filtration mechanisms and reversibility. *Environ Sci Technol* 42(22):8317–8323
- John G (1973) Rates of flocculation of latex particles by cationic polymers. *J Petrol Technol* 42(2):448–456
- Kanel S, Nepal D, Manning B, Choi H (2007) Transport of surface-modified iron nanoparticle in porous media and application to arsenic (III) remediation. *J Nanopart Res* 9(5):725–735
- Kang M, Baeg K-J, Khim D, Noh Y-Y, Kim D-Y (2014) Organic electronics: printed, flexible, organic nano-floating-gate memory: effects of metal nanoparticles and blocking dielectrics on memory characteristics. *Adv Funct Mater* 23(28):3482
- Kanj M (2013) Reservoir nanoagents for in-situ sensing and intervention. In: Mavroidis C, Ferreira A (eds) *Nanorobotics*. Springer, New York, pp 51–67
- Karimi A, Fakhrouiean Z, Bahramian A, Pour Khiabani N, Darabad JB, Azin R, Arya S (2012) Wettability alteration in carbonates using zirconium oxide nanofluids: EOR implications. *Energy Fuel* 26(2):1028–1036
- Krysmann MJ, Kellarakis A, Dallas P, Giannelis EP (2012) Formation mechanism of carbogenic nanoparticles with dual photoluminescence emission. *J Am Chem Soc* 134(2):747–750
- Lecoanet HF, Bottero J-Y, Wiesner MR (2004) Laboratory assessment of the mobility of nanomaterials in porous media. *Environ Sci Technol* 38(19):5164–5169
- Lee SW, Gallant BM, Byon HR, Hammond PT, Shao-Horn Y (2011) Nanostructured carbon-based electrodes: bridging the gap between thin-film lithium-ion batteries and electrochemical capacitors. *Energy Environ Sci* 4(6):1972–1985
- Lim Y-I, Jørgensen SB, Kim I-H (2005) Computer-aided model analysis for ionic strength-dependent effective charge of protein in ion-exchange chromatography. *Biochem Eng J* 25(2):125–140
- Lindlof JC, Stoffer KG (1983) A case study of seawater injection incompatibility. *J Petrol Technol* 35(7):7
- Ling XY, Phang IY, Vancso GJ, Huskens J, Reinhoudt DN (2009) Stable and transparent superhydrophobic nanoparticle films. *Langmuir* 25(5):3260–3263
- Liu X, He J (2008) Superhydrophilic and antireflective properties of silica nanoparticle coatings fabricated via layer-by-layer assembly and postcalcination. *J Phys Chem C* 113(1):148–152
- Menon MK, Zydney AL (1999) Effect of ion binding on protein transport through ultrafiltration membranes. *Biotechnol Bioeng* 63(3):298–307
- Mitragotri S (2013) Devices for overcoming biological barriers: the use of physical forces to disrupt the barriers. *Adv Drug Deliv Rev* 65(1):100–103
- Qian H, Pretzer LA, Velazquez JC, Zhao Z, Wong MS (2013) Gold nanoparticles for cleaning contaminated water. *J Chem Technol Biotechnol* 88(5):735–741
- Rodriguez E, Roberts MR, Yu H, Huh C, Bryant SL (2009) Enhanced migration of surface-treated nanoparticles in sedimentary rocks. In: SPE annual technical conference and exhibition, society of petroleum engineers, New Orleans, Louisiana, USA, SPE-124418-MS. doi:10.2118/124418-MS
- Saiers JE, Hornberger GM, Harvery C (1994) Colloidal silica transport through structured, heterogeneous porous media. *J Hydrol* 163:271–288
- Savage N, Diallo MS (2005) Nanomaterials and water purification: opportunities and challenges. *J Nanopart Res* 7(4):331–342
- Serres-Piole C, Preud'homme H, Moradi-Tehrani N, Allanic C, Jullia H, Lobinski R (2012) Water tracers in oilfield applications: guidelines. *J Petrol Sci Eng* 98–99:22–39
- Smallwood PV (1977) Some aspects of the surface chemistry of calcite and aragonite Part I: an electrokinetic study. *Colloid Polym Sci* 255(9):881–886
- Subramanian SK, Li Y, Cathles LM (2013) Nanoparticle transport through fractures and heterogeneous porous media. *Water Resour Res* 49(1):29–42
- van Krevel JWH, van Rutten JWT, Mandal H, Hintzen HT, Metselaar R (2002) Luminescence properties of terbium-, cerium-, or europium-doped α -sialon materials. *J Solid State Chem* 165(1):19–24
- Villamizar L, Lohateeraparp P, Harwell J, Resasco D, Shiau B (2013) Dispersion stability and transport of nanohybrids through porous media. *Transp Porous Media* 96(1):63–81
- Wippermann S, Vörös M, Rocca D, Gali A, Zimanyi G, Galli G (2013) High-pressure core structures of Si nanoparticles for solar energy conversion. *Phys Rev Lett* 110(4):046804
- Yu J, An C, Mo D, Liu N, Lee R (2012) Study of adsorption and transportation behavior of nanoparticles in three different porous media. In: The eighteenth SPE improved oil recovery symposium society of petroleum engineers, Tulsa, Oklahoma, USA, SPE-153337-MS. doi:10.2118/153337-MS
- Zeng R, Liu L, Li S, Zou Y, Zhang F, Yang Y, Cui H, Han E-h (2013) Self-assembled silane film and silver nanoparticles coating on magnesium alloys for corrosion resistance and antibacterial applications. *Acta Metall Sin* 26(6):681–686